Note: This copy is for your personal non-commercial use only. To order presentation-ready copies for distribution to your colleagues or clients, contact us at www.rsna.org/rsnarights.

RadioGraphics

Role of 3D CT in the Evaluation of the Temporal Bone[1]

Girish M. Fatterpekar, MD • Amish H. Doshi, MD • Mohit Dugar, MD
Bradley N. Delman, MD • Thomas P. Naidich, MD • Peter M. Som, MD

CME FEATURE

See accompanying test at http://www.rsna.org/education/rg_cme.html

LEARNING OBJECTIVES FOR TEST 6

After reading this article and taking the test, the reader will be able to:

- Describe the normal 3D anatomy of the temporal bone, including the morphologic features and interrelationships of individual structures.
- List the microanatomic structures of the temporal bone.
- Discuss the role of 3D CT in the evaluation of pathologic conditions of the temporal bone.

TEACHING POINTS

See last page

In recent years, three-dimensional (3D) multiplanar reformatted images from conventional cross-sectional computed tomographic (CT) data have been increasingly used to better demonstrate the anatomy and pathologic conditions of various organ systems. Three-dimensional volume-rendered (VR) CT images can aid in understanding the temporal bone, a region of complex anatomy containing multiple small structures within a relatively compact area, which makes evaluation of this region difficult. These images can be rotated in space and dissected in any plane, allowing assessment of the morphologic features of individual structures, including the small ossicles of the middle ear and the intricate components of the inner ear. The use of submillimeter two-dimensional reconstruction from CT data in addition to 3D reformation allows depiction of microanatomic structures such as the osseous spiral lamina and hamulus. Furthermore, 3D VR CT images can be used to evaluate various conditions of the temporal bone, including congenital malformations, vascular anomalies, inflammatory or neoplastic conditions, and trauma. The additional information provided by 3D reformatted images allows a better understanding of temporal bone anatomy and improves the ability to evaluate related disease, thereby helping to optimize surgical planning.

©RSNA, 2006

Abbreviations: EAC = external auditory canal, IAC = internal auditory canal, ICA = internal carotid artery, MPR = multiplanar reformatted, 3D = three-dimensional, 2D = two-dimensional, VR = volume rendered

RadioGraphics 2006; 26:S117–S132 • **Published online** 10.1148/rg.26si065502 • **Content Codes:** CT HN NR

[1]From the Department of Radiology, Mount Sinai Medical Center, One Gustave L. Levy Place, New York, NY 10029. Presented as an education exhibit at the 2005 RSNA Annual Meeting. Received January 26, 2006; revision requested March 7 and received March 23; accepted April 6. All authors have no financial relationships to disclose. **Address correspondence to** P.M.S. (e-mail: *Peter.Som@mssm.edu*).

©RSNA, 2006

Introduction

The temporal bone houses the middle ear, including the ossicles; the inner ear, which consists of the cochlea, vestibule, and semicircular canals; the bony canals for the facial and vestibulocochlear nerves; and the related vasculature and muscles. Conventional two-dimensional (2D) imaging has been used extensively to depict the individual structures of the temporal bone. However, the complex, multispatial orientation of these structures, contained as they are within a compact region, often makes it difficult to appreciate their three-dimensional (3D) orientation within the temporal bone and their intricate interrelationships. Recent developments in software technology have made it possible to rapidly generate 3D volumes from conventional 2D data (1–3). These volume-rendered (VR) images can be sectioned in any plane and rotated in space, allowing 3D insight into the anatomy of the temporal bone (4). Microanatomic structures that are not well seen with conventional 2D imaging can be clearly depicted using overlapping reconstruction at smaller intervals. In addition, the reformatted images provide complementary information about various conditions, including congenital malformations, vascular anomalies, inflammatory or neoplastic conditions, and trauma involving the temporal bone (5–7).

In this article, we discuss our retrospective study in terms of patients and procedures, review the normal anatomy of the temporal bone, and discuss and illustrate the utility of 3D computed tomography (CT) in demonstrating temporal bone anatomy and evaluating related disease.

Patients and Procedures

A retrospective study was performed that included 82 patients who had undergone high-resolution CT of the temporal bone for the evaluation of complaints related to the auditory system. Each scan was obtained on a 16-section spiral CT scanner (Somatom Sensation 16; Siemens Medical Solutions, Malvern, Pa). The studies were performed with the following parameters: 0.75-mm collimation, 0.75-mm section thickness, 120 kVp, 200 mAs, pitch of 0.8, a 15-cm field of view, and a 512 × 512 matrix. The initial data sets were then reconstructed at 0.1-mm intervals.

Teaching Point

During initial postprocessing, we observed that any amount of gantry tilt on the CT scanner caused distortion of 3D CT reformatted images. Therefore, 2D CT scans were obtained with a 0° gantry tilt and a scanning plane parallel to the inferior orbitomeatal line. In addition, overlapping submillimeter reconstruction of the raw data was performed to obtain the best possible 3D CT reformatted images.

Three-dimensional VR CT images were generated from the original 2D data with TeraRecon Aquarius Workstation v3.3 (TeraRecon, San Mateo, Calif). All reformatted images were obtained by a neuroradiology fellow or a postprocessing technologist. The application of different soft-tissue and bone algorithms to the 3D reformation permitted multiprojectional display of the various temporal bone structures, including the ossicles and the inner ear structures (eg, cochlea, vestibule, semicircular canals). With use of a built-in 3D cut-plane software technique, individual temporal bone structures were "removed" and analyzed, allowing optimal display of microanatomic components such as the delicate osseous spiral lamina of the cochlea. Three-dimensional reformatted images were also obtained from temporal bone scans to more effectively demonstrate disease.

Normal Anatomy

External Ear

The external ear consists of the auricle, or pinna, and the external auditory canal (EAC). The pinna collects sound waves, and the EAC conducts these vibrations to the tympanic membrane. The EAC forms an S-shaped curve as it extends from the auricle to the tympanic membrane. The medial two-thirds of the EAC is osseous and slightly narrower than the lateral third, which is cartilaginous. A somewhat more pronounced constriction, the isthmus, is seen at the bone-cartilage junction (Fig 1). The narrowing of the osseous segment of the EAC results in the amplification of sound waves as they progress to the tympanic membrane. The tympanic membrane marks the medial boundary of the EAC, separating the external ear from the tympanic cavity (8–11).

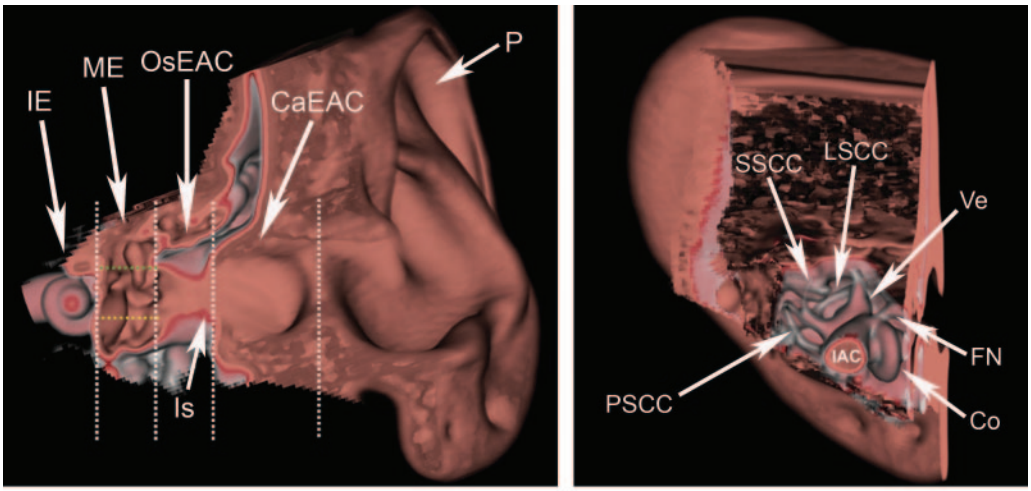

a. b.

Figure 1. Normal anatomy of the auditory apparatus. **(a)** Oblique coronal 3D VR CT image (anterior view) shows the pinna *(P)*; the EAC, including the cartilaginous *(CaEAC)* and osseous *(OsEAC)* portions; the isthmus *(Is)*; the middle ear cavity *(ME)*; and the inner ear *(IE)*. The middle ear is divided into the epitympanum (above dotted green line), mesotympanum (between dotted green and dotted yellow lines), and hypotympanum (below dotted yellow line). **(b)** Three-dimensional VR CT image (view from the dissected medial portion of the temporal bone) shows the inner ear, including the cochlea *(Co)*, vestibule *(Ve)*, superior semicircular canal *(SSCC)*, lateral semicircular canal *(LSCC)*, and posterior semicircular canal *(PSCC)*. The internal auditory canal *(IAC)* and the bony canal for the facial nerve *(FN)* are also seen.

Middle Ear

The tympanic cavity, or middle ear, can be structurally divided into three parts. The tympanic cavity proper (mesotympanum) lies at the level of and directly opposite the tympanic membrane; the epitympanic recess (attic) lies above the level of the tympanic membrane; and the hypotympanum, as its name suggests, lies inferior to the tympanic membrane (Fig 1). The tympanic cavity houses three ossicles: the malleus, the incus, and the stapes. The ossicular chain transmits and amplifies vibrations incident on the tympanic membrane across the middle ear cavity, causing deflection of the oval window, which is attached to the footplate of the stapes (8,9,11).

The malleus, which is the largest of the ossicles, lies anterolateral to the incus and stapes. A facet on the posterior surface of the head of the malleus articulates with the body of the incus. The head of the malleus and the body of the incus articulate by means of a thin capsular ligament, forming a diarthrodial joint. A mild constriction, the neck of the malleus, is seen at the inferior aspect of the club-shaped head and provides attachment to the tensor tympani. More inferiorly lies the long process, or manubrium, of the malleus. The tip of the manubrium attaches to the tympanic membrane at the umbo (8–10). Small bony spicules, the anterior and lateral processes, project from the upper portion of the manubrium and provide attachment for the anterior and lateral malleal ligaments, which help support the malleus within the middle ear cavity (Fig 2) (8,9,12).

The incus is shaped somewhat like a premolar tooth, with two widely diverging processes that differ in length. A facet on the anterior surface of the body of the incus articulates with the head of the malleus. The short process of the incus is directed posterolaterally; the long process is directed inferiorly and lies parallel to the manubrium of the malleus (8,9). The tip of the long process bends medially to end in a rounded projection, the lenticular process, which articulates with the stapes (Fig 3) (8,13).

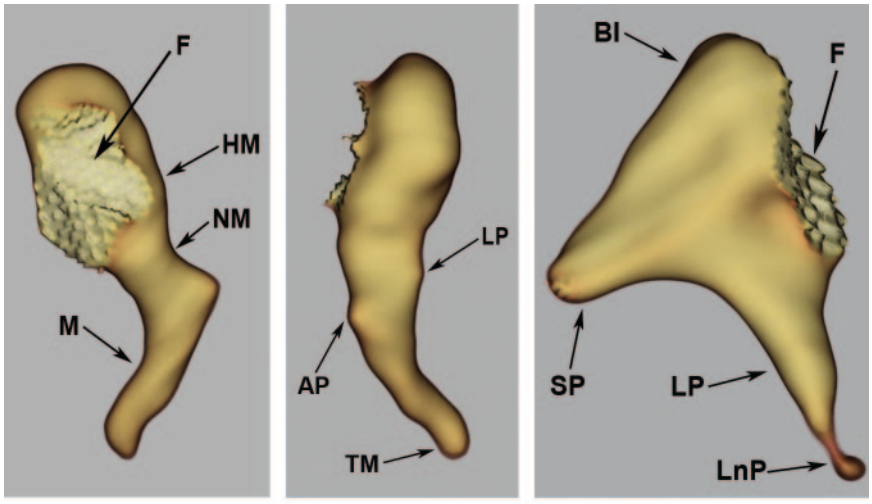

2a. 2b. 3.

Figures 2, 3. **(2)** Normal anatomy of the malleus. **(a)** Posterior oblique 3D VR CT image shows the head of the malleus *(HM)* and, appearing as a narrow constriction inferiorly, the neck of the malleus *(NM)*. The manubrium *(M)* lies inferior to the neck. The head of the malleus demonstrates a facet *(F)* on its posterior aspect that articulates with the body of the incus. **(b)** Anterior oblique 3D VR CT image shows two bony spicules arising from the upper portion of the manubrium, the anterior process *(AP)* and the lateral process *(LP)*. The tip of the manubrium *(TM)* attaches to the tympanic membrane at the umbo. **(3)** Normal anatomy of the incus. Three-dimensional VR CT image (inferolateral view) shows the body of the incus *(BI)*, which demonstrates a facet *(F)* on its anterior surface that articulates with the head of the malleus. The short process *(SP)* is directed posterolaterally, and the long process *(LP)* is directed inferiorly. The tip of the long process bends medially to end in a rounded projection, the lenticular process *(LnP)*, which articulates with the head of the stapes.

The stapes is the most medial ossicle. It resembles a stirrup and consists of a head, a neck, two crura, and a footplate. The head articulates with the lenticular process of the incus. Inferior to the head lies the neck, which, at its posterior aspect, provides insertion to the tendon of the stapedius muscle. Two crura, the anterior and posterior crura, diverge from the neck and are connected at their inferior ends by the footplate. The footplate sits on the oval window, attached to its margins by the annular ligament (Fig 4) (8,9,11).

Teaching Point

The surface area of the tympanic membrane is up to 30 times greater than that of the oval window. Thus, the pressure exerted on the tympanic membrane by a sound wave is concentrated through the ossicles onto the much smaller area of the oval window, resulting in a pressure increase and amplification of sound transmission. A lever mechanism that exists between the ossicles further contributes to sound amplification.

This amplification that occurs within the tympanic cavity is crucial for overcoming the inertia of the perilymph within the osseous labyrinth in the inner ear (8,9).

Inner Ear

The inner ear consists of the bony labyrinth, which lies within the petrous portion of the temporal bone and is the densest structure in the entire human body (Fig 1). The bony labyrinth contains the membranous labyrinth, a complex interconnected series of membranous sacs and ducts that are primarily responsible for balance and hearing. Fluid within the bony labyrinth called the perilymph surrounds the membranous labyrinth, which contains its own unique fluid, the endolymph (11).

The bony labyrinth consists of three structures: the cochlea, the vestibule, and the semicircular canals (Fig 5). The cochlea is shaped like a conical snail shell. It consists of a bony canal wound around a conical central core called the modiolus. The canal winds around this central axis slightly more than 2½ times and gradually decreases in

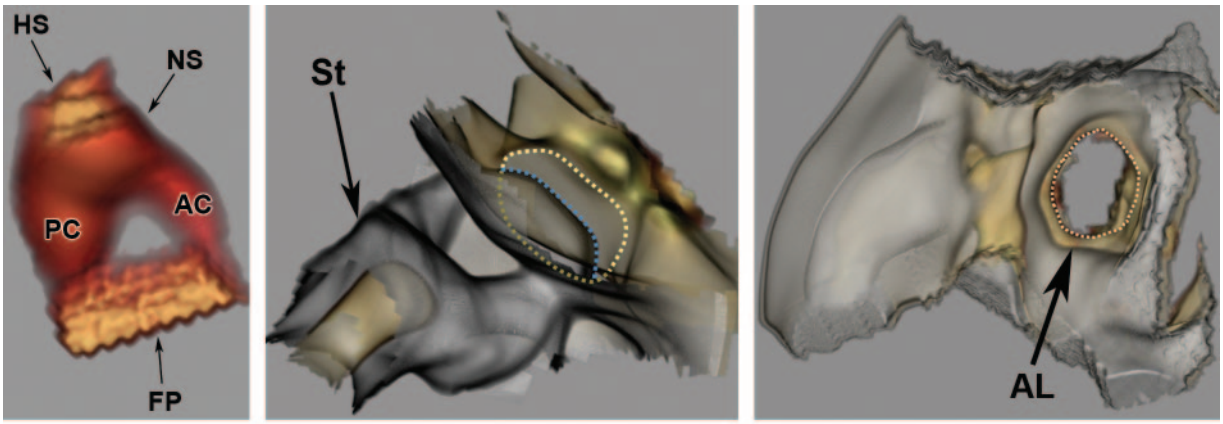

Figure 4. Normal anatomy of the stapes. **(a)** Three-dimensional VR CT image (inferior view) shows the head of the stapes *(HS)*, which articulates with the lenticular process of the incus. Inferior to the head of the stapes is the stapes neck *(NS)*, which provides attachment to the stapedius muscle. The anterior crus *(AC)* and posterior crus *(PC)* connect the stapes neck to the stapes footplate *(FP)*. The stapes is a cartilaginous structure, unlike the bony malleus and incus. Therefore, the color rendering of the stapes on the 3D shaded-surface-display reformatted images was different from that of the malleus and incus (cf Figs 2, 3). **(b, c)** Three-dimensional VR CT images (view from the dissected tympanic cavity looking into the oval window) obtained with **(b)** and without **(c)** the stapes *(St)* present show that the stapes footplate (dotted blue line) sits on the oval window (dotted yellow line), attached to its margins by the annular ligament *(AL)*.

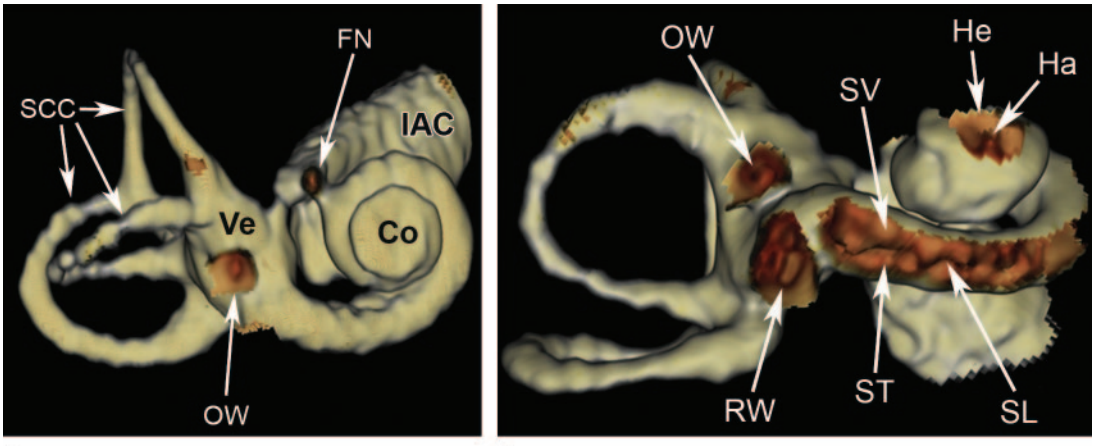

Figures 5, 6. **(5)** Normal anatomy of the bony labyrinth. Three-dimensional VR CT image (anterolateral view) shows the normal bony labyrinth, which consists of the cochlea *(Co)*, vestibule *(Ve)*, and semicircular canals *(SCC)*. *FN* = facial nerve canal, *IAC* = internal auditory canal, *OW* = oval window. **(6)** Normal anatomy of the cochlea. Three-dimensional VR CT image (inferolateral view after dissection of a portion of the inferior wall of the cochlea) shows the osseous spiral lamina *(SL)*, which divides the bony canal for the cochlea into upper and lower passages, the scala vestibule *(SV)* and the scala tympani *(ST)*, respectively. Dissection of the apical cochlear bony labyrinth shows the terminus of the spiral lamina as a conical projection, or hamulus *(Ha)*, allowing free communication between the scala vestibule and the scala tympani at the helicotrema *(He)*. *OW* = oval window, *RW* = round window.

diameter as it spirals toward the apex. A delicate osseous spiral lamina projects from the modiolus and divides the bony canal for the cochlea into an upper passage (scala vestibuli) and a lower passage (scala tympani). Between these two scalae lies the cochlear duct, or scala media, which contains the organ of Corti, the sensory organ of hearing. At the apex of the cochlea, the osseous spiral lamina ends freely in a hook-shaped hamulus, which partly bounds the helicotrema, an opening through which the two scalae communicate (Fig 6) (8,9,11).

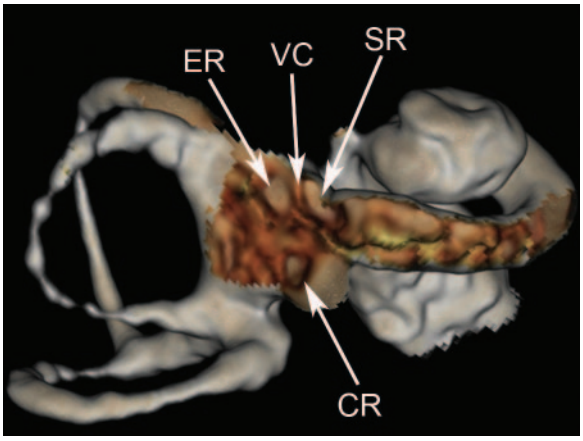

Figure 7. Normal anatomy of the vestibule. Three-dimensional VR CT image (inferolateral view after dissection of the lateral wall of the vestibule) demonstrates the elliptical recess *(ER)* posteriorly and the spherical recess *(SR)* anteriorly, which house the utricle and saccule, respectively. A bony ridge, the vestibular crest *(VC)*, lies between the elliptical and spherical recesses. The vestibular crest divides inferiorly into two limbs that form an inverted V and bound a small depression, the cochlear recess *(CR)*. The cochlear recess houses the blind opening of the cochlear duct.

The vestibule is the central and most capacious portion of the bony labyrinth. The vestibule is continuous anteriorly with the cochlea and posteriorly with the semicircular canals. It contains the utricle and the saccule, parts of the membranous labyrinth, which are primarily involved with balance. Superiorly and posteriorly on the medial wall of the vestibule is the elliptical recess, which houses the utricle; inferiorly and anteriorly lies the spherical recess, which accommodates the saccule. Between these two recesses is an oblique ridge, the vestibular crest, which divides posteriorly into two limbs bounding a small depression, the cochlear recess. The cochlear recess in turn houses the blind opening of the cochlear duct (Fig 7) (8,9,11).

There are three semicircular canals: superior, posterior, and lateral. The planes of the semicircular canals are nearly orthogonal, or at right angles, to each other. Each of the canals forms about two-thirds of a circle and is enlarged anteriorly to form the ampulla (8,9,14). The posterior end of the superior semicircular canal joins the upper end of the posterior semicircular canal to form a common limb known as the common crus. The perilymphatic space of each semicircular canal opens into and communicates freely with that of the vestibule (8,9). The osseous semicircular canals contain the corresponding membranous semicircular ducts, which are part of the membranous labyrinth and communicate with the utricle.

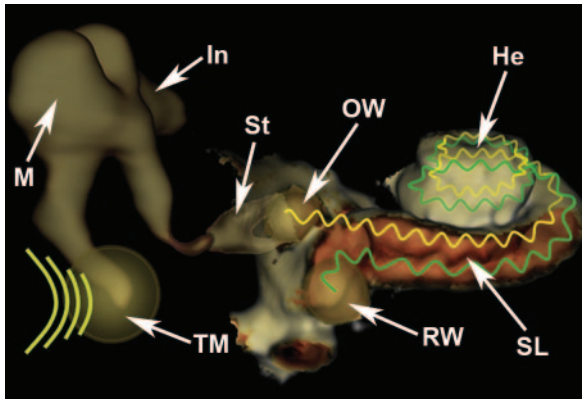

Figure 8. Sound transmission. Three-dimensional VR CT image demonstrates the anatomic structures involved in the transmission of sound. Sound vibrations transmitted through the tympanic membrane *(TM)* are amplified multifold across the middle ear cavity by the lever mechanism of the ossicles. In addition, the disproportionately larger size of the tympanic membrane allows sound waves to be concentrated onto the smaller oval window *(OW)*, further contributing to sound augmentation. Inward deflection of the oval window by the footplate of the stapes *(St)* compresses the fluid in the scala vestibuli (wavy yellow line). This compression wave travels along the coils of the cochlea in the scala vestibuli to the helicotrema *(He)*. It then spirals back through the scala tympani (wavy green line) to the round window *(RW)*, which serves as a pressure-relief diaphragm. The vibrations in the scala vestibuli also stimulate the cochlear duct (lying adjacent to the osseous spiral lamina *[SL]*), where mechanical energy is converted into electrical impulses and transmitted via the cochlear nerve to the brainstem (not shown). *In* = incus, *M* = malleus.

Collectively, the semicircular ducts are responsible for the detection of angular acceleration (8,9,14).

Sound vibrations traveling through the ossicular chain in the tympanic cavity deflect the oval window through its attachment to the footplate of the stapes. This deflection of the oval window compresses the perilymph in the scala vestibuli. Vibrations in the perilymph are transmitted to the endolymph in the cochlear duct, which contains the spiral organ of Corti. Sound transduction occurs within the organ of Corti, where mechanical energy is converted into electrical impulses. These electrical impulses are in turn transmitted by the cochlear nerve to the brainstem. Simultaneously, the compression waves within the scala vestibuli travel along the coils of the cochlea to the helicotrema. The compression waves are transmitted through this opening and travel back down the coils in the scala tympani to reach the round window. The round window serves as a pressure-relief diaphragm, bulging outward with each pressure wave in the scala tympani (Fig 8) (8,9).

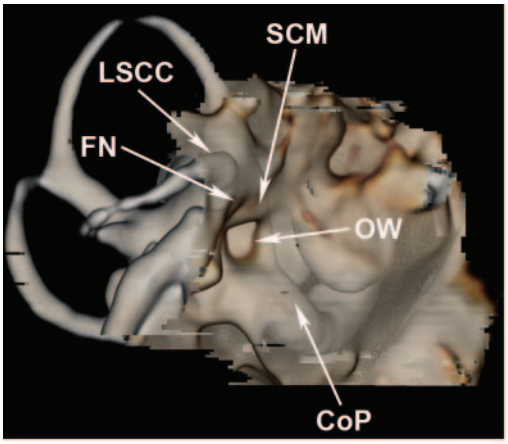

9.

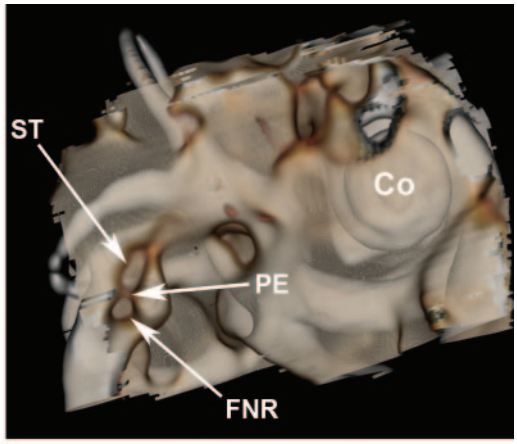

10.

Figures 9, 10. **(9)** Three-dimensional VR CT image (semiopaque windowing) shows the inner ear impressions produced on the medial wall of the tympanic cavity. The prominence produced by the anterior limb of the lateral semicircular canal *(LSCC)* is seen posteriorly, and the prominence produced by the facial nerve canal *(FN)* is seen anteriorly. The prominence produced by the curved terminus of the septum canalis musculotubari *(SCM)* is seen superior and anterior to the oval window *(OW)*. The septum canalis musculotubari serves as the landmark for the geniculate ganglion. The prominence produced by the cochlear promontory *(CoP)* lies inferior and slightly anterior to the oval window. **(10)** Three-dimensional VR CT image (semiopaque windowing) shows two recesses on the posterior wall of the tympanic cavity: The sinus tympani *(ST)* lies medial to the facial nerve recess *(FNR)* and indicates the position of the ampulla of the posterior semicircular canal. The pyramidal eminence *(PE)* is a small conical projection located between the two recesses that gives rise to the stapedius muscle. *Co* = cochlea.

Medial and Posterior Walls of the Tympanic Cavity

The inner ear structures produce multiple impressions, or ridges, on the medial and posterior walls of the tympanic cavity. With use of semiopaque windowing and careful dissection of overlying structures, these impressions can be clearly visualized on 3D VR images.

Posteriorly and superiorly along the medial wall of the tympanic cavity is the prominence produced by the anterior limb of the lateral semicircular canal. Inferior to this prominence and extending more anteriorly is the prominence of the bony canal for the facial nerve. Anterior to the prominence of the bony canal for the facial nerve is the curved terminus of the septum canalis musculotubari, which serves as a landmark for the geniculate ganglion. Immediately inferior to this prominence is the oval window. Inferior and slightly anterior to the oval window lies the rounded promontory, a convexity produced by the basal turn of the cochlea (Fig 9) (8,9).

The posterior wall of the tympanic cavity contains two important recesses: the sinus tympani and the facial nerve recess. The sinus tympani indicates the position of the ampulla of the posterior semicircular canal. Lateral to the sinus tympani is the facial nerve recess, an important surgical landmark when entrance into the tympanic cavity is gained using the mastoid approach. Entrance is initially gained into the middle ear cavity by enlarging the facial nerve recess using the facial nerve and chorda tympani as landmarks (8,10, 15). The pyramidal eminence is situated between the sinus tympani and the facial nerve recess. This eminence gives rise to the stapedius muscle (Fig 10) (8–10).

Osseous Neural Canals for the Facial and Vestibulocochlear Nerves

The internal auditory canal (IAC) traverses the petrous portion of the temporal bone and functions as a conduit for the facial and vestibulocochlear nerves as they course from the brainstem to the inner ear. The medial opening of the IAC is known as the porus acusticus. The lateral end of the IAC, known as the fundus, is separated from the inner ear by a vertical plate of bone that is perforated to allow passage of the facial and vestibulocochlear nerves. The fundus is divided into upper and lower portions by a horizontal ridge of bone known as the falciform crest. A thin vertical crest of bone known as the Bill bar further divides the upper portion of the fundus into an anterior opening for the facial nerve and a posterior opening for the superior vestibular nerve (Fig 11). The superior vestibular nerve innervates the utricle and the superior and lateral semicircular

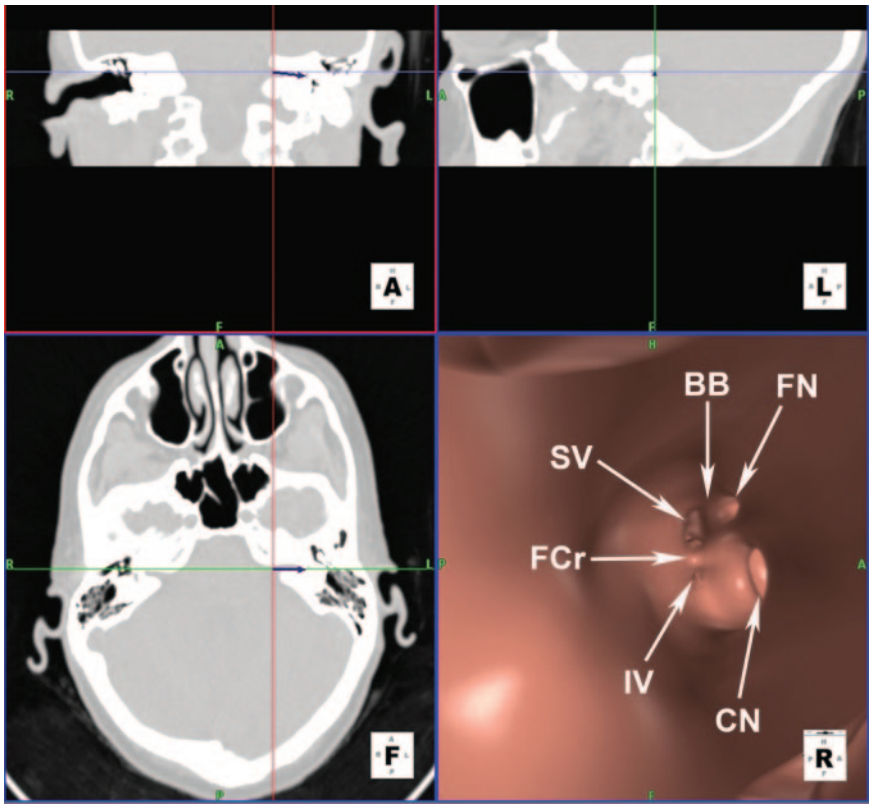

Figure 11. Normal IAC. Coronal (top left), sagittal (top right), and axial (bottom left) VR CT images show the normal IAC (arrow). Virtual IAC otoscopic image (bottom right) shows the fundus of the IAC, which is divided into upper and lower portions by the falciform crest *(FCr)*. The Bill bar *(BB)* further subdivides the upper portion of the fundus into openings for the facial nerve *(FN)* anteriorly and the superior vestibular nerve *(SV)* posteriorly. The lower portion of the fundus contains an anterior opening for bundles of the cochlear nerve *(CN)* and a pinpoint posterior opening for the inferior vestibular nerve *(IV)*.

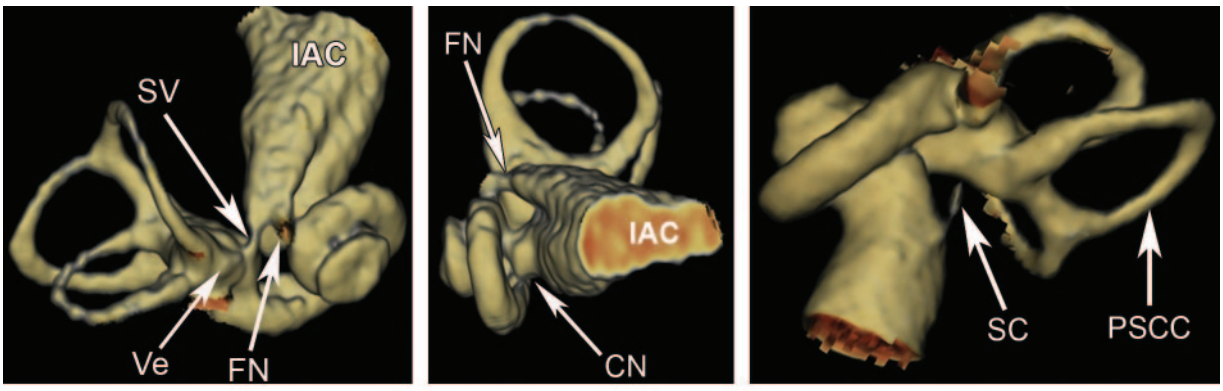

12. 13. 14.

Figures 12–14. **(12)** Normal anatomy of the osseous neural canals for the facial and superior vestibular nerves. Three-dimensional VR CT image (superior view) shows the bony canal for the facial nerve *(FN)* dissected in its proximal portion at the anterosuperior aspect of the internal auditory canal *(IAC)*. The bony canal for the superior vestibular nerve *(SV)* lies posterior to the facial nerve canal and extends to the vestibule *(Ve)*. **(13)** Normal anatomy of the osseous neural canals for the facial and cochlear nerves. Three-dimensional VR CT image (medial view) shows that the cochlear nerve canal *(CN)* lies inferior to the facial nerve canal *(FN)* and courses to the cochlea. *IAC* = internal auditory canal. **(14)** Singular canal. Three-dimensional VR CT image (posteroinferior view) shows the singular canal *(SC)*, through which courses a branch of the inferior vestibular nerve. The inferior vestibular nerve innervates the posterior semicircular canal *(PSCC)*.

canals (Fig 12). The lower compartment of the fundus of the IAC has a rounded opening anteriorly through which the bundles of the cochlear division of the eighth cranial nerve pass to innervate the cochlea (Fig 13). The lower compartment has a pinpoint opening posteriorly for the passage of the inferior vestibular nerve, which

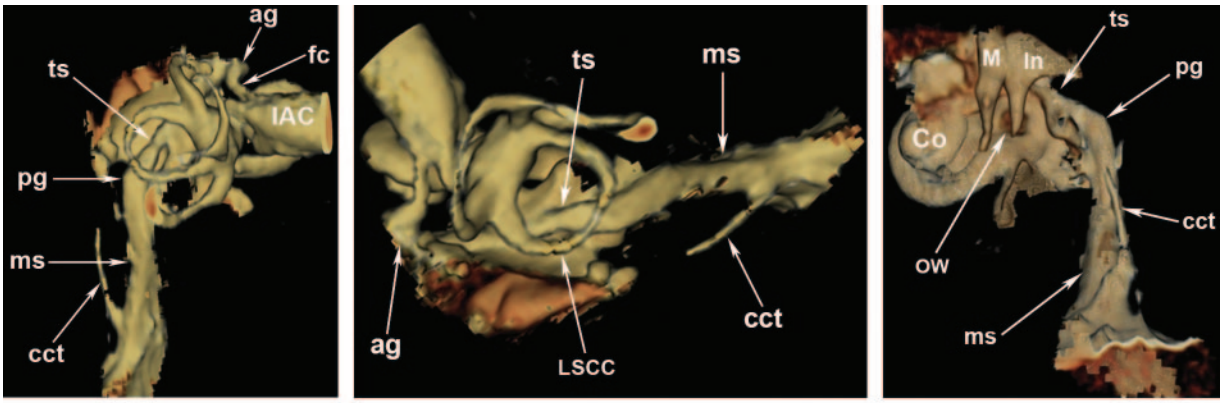

a. b. c.

Figure 15. Normal anatomy of the facial nerve canal. Three-dimensional VR CT images (posterior **[a]**, superior **[b]**, and lateral **[c]** views) show the course of the facial nerve through its bony canal as it exits the anterosuperior aspect of the fundus of the internal auditory canal *(IAC)*. The labyrinthine segment of the facial nerve courses through the fallopian canal *(fc)* to the geniculate ganglion, where the nerve makes a hairpin turn known as the anterior genu *(ag)*. The tympanic segment *(ts)* of the facial nerve canal runs below the lateral semicircular canal *(LSCC)* and above the oval window *(OW)* along the medial wall of the tympanic cavity. It then makes a gentle curve (the posterior genu *[pg]*) and heads vertically downward as the mastoid segment *(ms)* to exit the temporal bone at the stylomastoid foramen. The chorda tympani arises from the lateral aspect of the mastoid segment approximately 5 mm proximal to the stylomastoid foramen and courses superiorly within its own bony canal, the canaliculus chorda tympani *(cct)*. *Co* = cochlea, *In* = incus, *M* = malleus.

innervates the saccule. In addition, the inferior vestibular nerve gives off a branch within the IAC that arises approximately 3 mm proximal to the fundus and courses within its own bony canal, the singular canal, to innervate the posterior semicircular canal (Fig 14) (8–10,16). As illustrated in Figure 11, of the four neural openings identified at the fundus of the IAC, the opening for the cochlear nerve is the largest and that for the inferior vestibular nerve is the smallest (17,18).

Facial Nerve Canal

The facial nerve takes a winding path through the temporal bone, and its course is divided into three basic segments: the labyrinthine, the tympanic, and the mastoid segments (Fig 15). With use of multiprojectional 3D VR CT images, we were able to demonstrate the course of the facial nerve within the temporal bone.

The labyrinthine segment of the facial nerve emerges from the anterosuperior aspect of the IAC, coursing anterolaterally within its own bony channel, the fallopian canal. This segment of the facial nerve is relatively short, measuring 3–4 mm, and lies superior to the cochlea. It makes a subtle anteromedial turn as it courses anteriorly to reach the geniculate ganglion. At the ganglion, the facial nerve reverses its direction, making a sharp posteroinferior turn to continue as the tympanic segment. This sharp turn, known as the anterior genu, lies superomedial to the cochlear promontory. The tympanic segment is approximately 12 mm long and extends from the geniculate ganglion to the posterior genu. This portion of the facial nerve courses posteriorly along the medial wall of the tympanic cavity, just inferior to the lateral semicircular canal and superior to the oval window, to reach the sinus tympani. At the sinus tympani, the facial nerve again changes direction, making a gentler posteroinferior turn to form the posterior genu. Here, the facial nerve assumes a more vertical position and descends just behind the posterior wall of the tympanic cavity as the mastoid segment to exit the temporal bone through the stylomastoid foramen. The mastoid segment is the longest portion of the intratemporal facial nerve, measuring approximately 15–20 mm. The chorda tympani arises from the lateral aspect of the mastoid segment of the facial nerve approximately 5 mm superior to the stylomastoid foramen and follows a subtle curved course superoanteriorly in the canaliculus chorda tympani (Fig 15). It then proceeds anteriorly within the tympanic cavity, exiting the temporal bone through a minute canal, the anterior canaliculus, near the petrotympanic fissure. It joins the lingual nerve to supply taste sensation to the anterior two-thirds of the tongue (8–11,19).

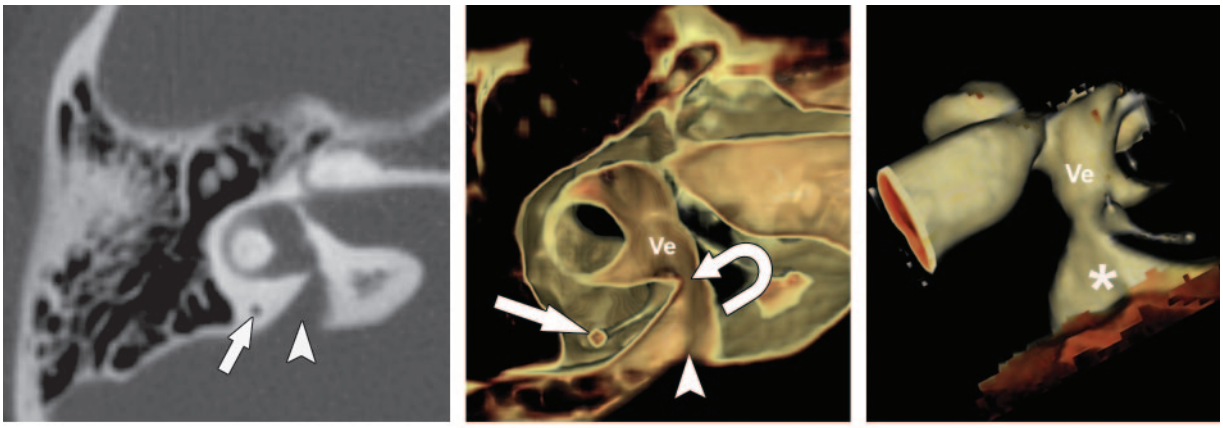

a. b. c.

Figure 16. Large vestibular aqueduct syndrome in a 9-year-old girl with progressive sensorineural hearing loss. **(a)** CT scan shows a dilated vestibular aqueduct (arrowhead). The normal vestibular aqueduct should be approximately the same size as the posterior semicircular canal (arrow). **(b)** Corresponding 3D CT reformatted image again demonstrates the dilated vestibular aqueduct (arrowhead). The opening of the vestibular aqueduct (curved arrow) into the vestibule *(Ve)* is also seen. Straight arrow indicates the posterior semicircular canal. **(c)** Three-dimensional VR CT image (posterior view) shows the classic funnel-shaped deformity of the dilated vestibular aqueduct (*) resulting from an enlarged endolymphatic sac housed within the dorsal portion of the vestibular aqueduct. *Ve* = vestibule.

Temporal Bone Disease

Congenital Malformations

Large Vestibular Aqueduct Syndrome.—The vestibular aqueduct is a curvilinear tubular structure that extends from the posteroinferior surface of the temporal bone to the medial wall of the vestibule. It contains the endolymphatic sac, which is connected to the utricle and saccule by the endolymphatic duct. The vestibular aqueduct normally measures less than 1.5 mm in diameter and approximates the size of the posterior semicircular canal, which runs anterior and parallel to the aqueduct (8,20,21). The exact physiologic role of the vestibular aqueduct is not known. However, a dilated vestibular aqueduct has been increasingly recognized as being directly related to sensorineural hearing loss (8,22,23). In a study by Arcand et al (24), large vestibular aqueduct syndrome was present in approximately 12% of children who presented with congenital sensorineural hearing loss.

Teaching Point

A dilated vestibular aqueduct can be easily recognized at conventional cross-sectional imaging by identifying its abnormal size in relation to the adjacent posterior semicircular canal. However, 3D multiplanar reformatted (MPR) CT images can more clearly demonstrate the classic funnel-shaped deformity of the dilated vestibular aqueduct, which occurs due to an enlarged endolymphatic sac housed within the dorsal vestibular aqueduct (Fig 16) (8). Thus, 3D CT allows better display of underlying disease.

Congenital Ossicular Malformation with Oval Window Atresia.—Conductive hearing loss in the pediatric population is usually due to an acquired condition such as acute or chronic otitis media. Congenital causes of conductive hearing loss in children are relatively uncommon. Most cases of congenital conductive hearing loss are secondary to atresia or stenosis of the EAC or, less frequently, to malformed ossicles (25). Absence of the oval window has been suggested as an even more uncommon cause (25–27). Recent advances in imaging techniques, such as submillimeter reconstruction and 3D VR multiplanar imaging, have markedly improved the evaluation of congenital anomalies that cause conductive hearing loss. To obtain the best possible surgical outcome, it is vital for the neuro-otologist or otolaryngologist to appreciate the full extent of congenital anomalies present. It is therefore imperative that the radiologist demonstrate the underlying anomalies in the greatest possible detail, thereby allowing optimal presurgical planning.

Teaching Point

Figure 17 illustrates congenital ossicular malformation in a young boy. In this case, the congenitally malformed ossicles were easily identified at routine cross-sectional imaging; however, the atretic right oval window could be clearly depicted only with 3D VR images. This additional information is crucial for the clinician because

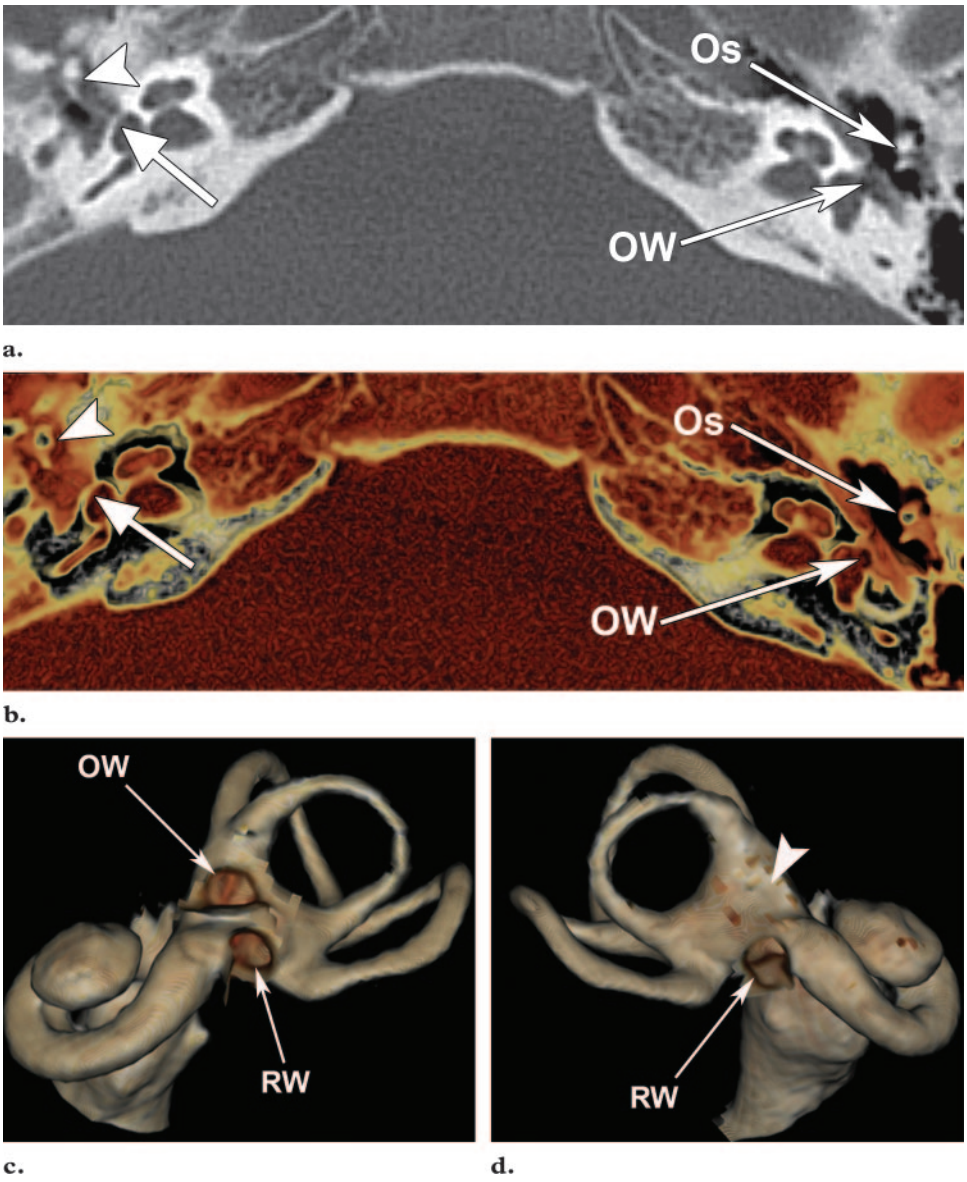

Figure 17. Congenital ossicular malformation with oval window atresia in a 12-year-old boy with right-sided mixed hearing loss. **(a, b)** CT scan **(a)** and corresponding 3D CT reformatted image **(b)** show malformed ossicles with an associated soft-tissue mass (arrowhead) attached to the lateral wall of the right tympanic cavity. A suspicious platelike covering (arrow) is seen in the expected region of the right oval window. The left-sided ossicles *(Os)* and left oval window *(OW)* are normal. **(c)** Three-dimensional VR CT image (inferolateral view) shows a normal left bony labyrinth with the oval window *(OW)* and round window *(RW)* well depicted. **(d)** Three-dimensional VR CT image (inferolateral view) shows an abnormal right bony labyrinth with absence of the oval window (arrowhead). *RW* = round window.

simply addressing the problem of malformed ossicles is not sufficient to correct the hearing loss; surgical repair of the atretic oval window is also necessary (28,29). Thus, 3D MPR CT images allow a more complete and thorough evaluation of congenital anomalies, which aids in presurgical planning.

Vascular Anomalies

An aberrant course of the internal carotid artery (ICA) inside the temporal bone is a rare occurrence (30). However, it is crucial to recognize this entity, which can easily be misdiagnosed as a neoplastic process (eg, paraganglioma) or an inflammatory condition (eg, effusive otitis media). Subsequent tympanotomy or biopsy of this "mass" can result in catastrophic hemorrhage. Aberrant ICA may manifest as pulsatile tinnitus, hearing loss, vertigo, or a sensation of fullness in the ear (8,31–33).

Conventional CT with complementary 3D reformation is excellent for the evaluation of aberrant ICA. The axial and coronal 2D CT scans in Figure 18a and 18b demonstrate bilateral aberrant carotid arteries. However, by using 3D MPR CT images (Fig 18c–f), we were able to show a band of tissue attaching the malleus to the aberrant left ICA, accounting for more severe tinnitus on the left side. Unlike conventional 2D images, 3D VR CT images can be rotated in space and in any plane, an advantage that allows a more complete evaluation of the underlying disease.

Figure 18. Aberrant ICAs in a 26-year-old woman with bilateral tinnitus, which was more pronounced in the left ear. **(a, b)** CT scans of the right **(a)** and left **(b)** temporal bones show bilateral aberrant ICAs (*). The manubrium of the left malleus (arrow in **b**) was identified only retrospectively, after evaluation of the 3D VR CT images (cf **c, d**), as being in proximity to the aberrant left ICA. **(c, d)** Corresponding 3D VR CT images also demonstrate the bilateral aberrant ICAs (*). The manubrium of the left malleus (arrow in **d**) appears to be attached to the aberrant left ICA. On the contralateral side, the right malleus (arrowhead in **c**) is not as close to the aberrant right ICA. **(e)** Three-dimensional VR CT image (lateral view) shows the aberrant right ICA (*). There is no attachment of the malleus *(M)* to the artery. *In* = incus. **(f)** Three-dimensional VR CT image (lateral view) clearly demonstrates attachment of the abnormally long manubrium of the left malleus *(M)* to the aberrant left ICA (*) by a band of soft tissue (arrow). *In* = incus.

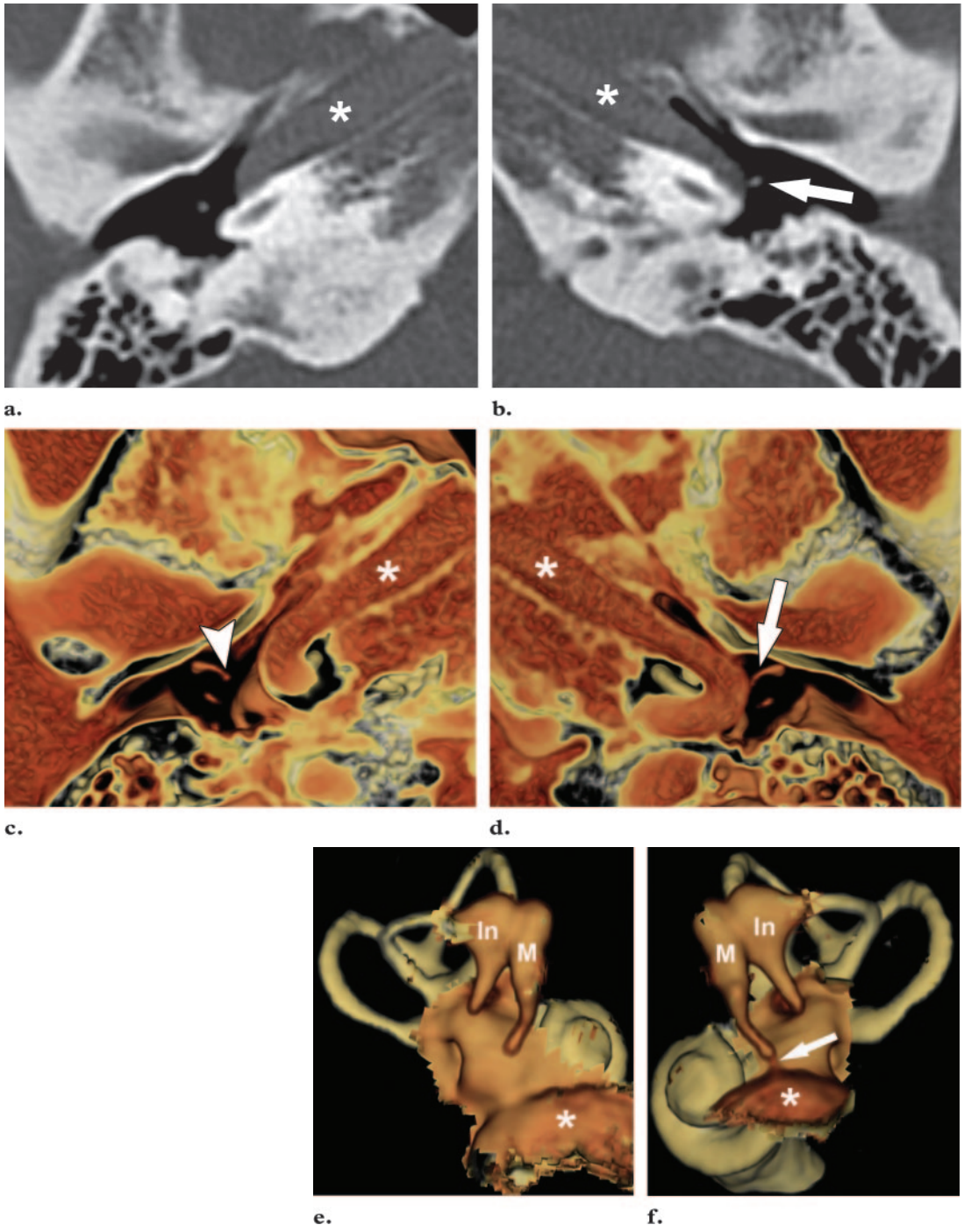

Figure 19. Cholesteatoma in a 26-year-old woman with right-sided hearing loss. **(a, b)** CT scan **(a)** and corresponding 3D CT reformatted image **(b)** show erosion of the right malleus and incus (arrow). The stapes *(St)* is intact and is better appreciated on the 3D image. The left malleus and incus (arrowhead) are normal. **(c)** Three-dimensional VR CT image (lateral view after dissection of the anteroinferior portion of the EAC) shows pressure erosion of the head of the right malleus *(Me)* and the body of the incus *(BIe)*, along with nearly complete erosion of the short process of the incus *(SPe)*. Extension of the erosion into the incudomalleolar articulation *(IMe)* is also noted. **(d)** Three-dimensional VR CT image (lateral view after dissection of the anteroinferior portion of the EAC) shows the normal left side for comparison. *IM* = incudomalleolar articulation, *In* = incus, *M* = malleus, *SP* = short process of the incus.

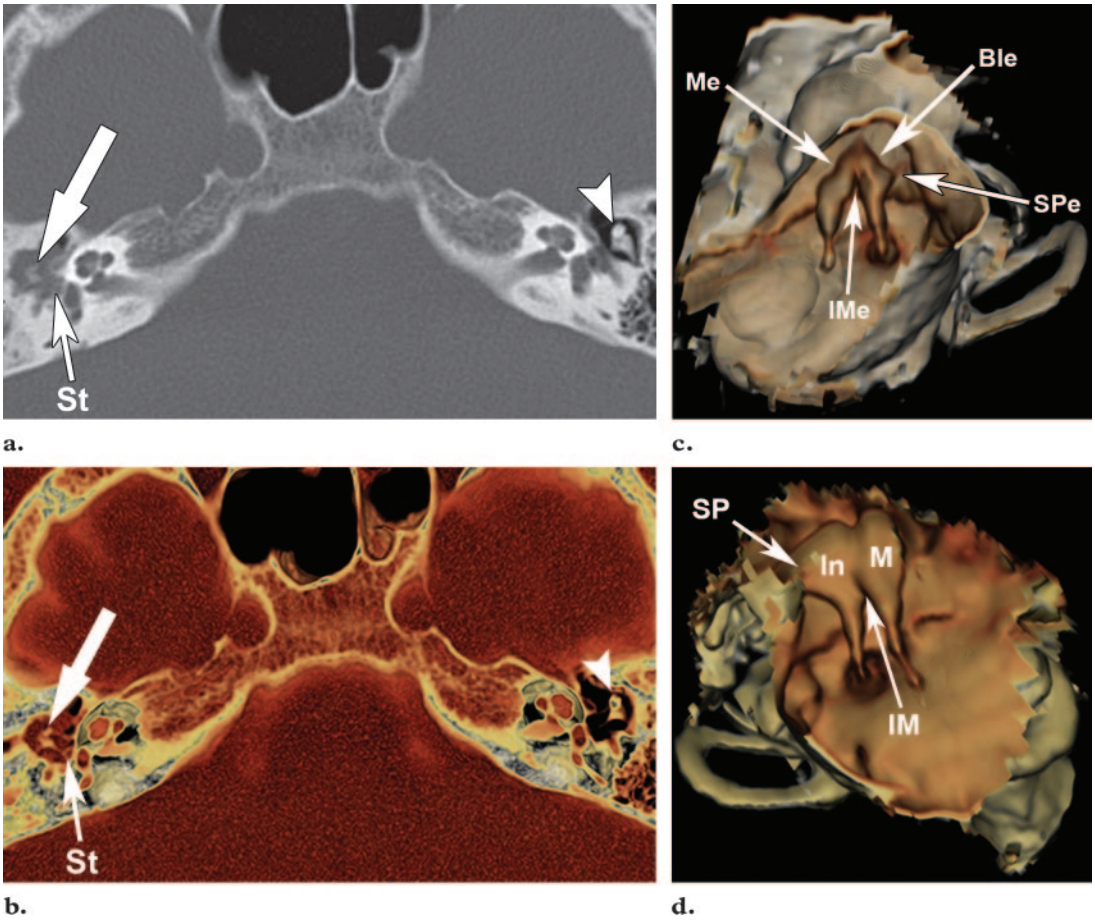

Inflammatory or Neoplastic Conditions

Cholesteatomas are erosive collections of keratinous debris arising from an ingrowth of stratified squamous epithelium. Cholesteatomas can be acquired or congenital in origin. Acquired middle ear cholesteatoma is the most common type, accounting for 98% of cases (8,10). At CT, cholesteatomas classically manifest as a soft-tissue mass causing underlying bone erosion (34–36). There are various types of surgeries for the treatment of cholesteatomas, including simple, modified radical, and radical mastoidectomies. The type of surgery performed depends on the extent of disease, which is directly related to the extent of the underlying erosions. Therefore, detailed preoperative radiologic assessment of the cholesteatoma is important (8,37).

Teaching Point

Figure 19 illustrates cholesteatoma in a woman with right-sided hearing loss. This case demonstrates that, although the diagnosis of cholesteatoma is readily established with conventional CT (Fig 19a), the full extent of the underlying erosions can be established only by using 3D VR CT images (Fig 19c, 19d). More specifically, extension of the erosive process into the incudomalleolar joint could be evaluated only on 3D reformatted images in this case. In addition, the stapes, due to its cartilaginous skeleton, can at times be partially masked by the surrounding cholesteatoma at conventional CT, thus precluding its complete evaluation. As Figure 19 demonstrates, the use of 3D CT reformatted images with varying thicknesses helps better assess the integrity of the stapes. Such additional information greatly improves presurgical evaluation and allows more appropriate surgical planning.

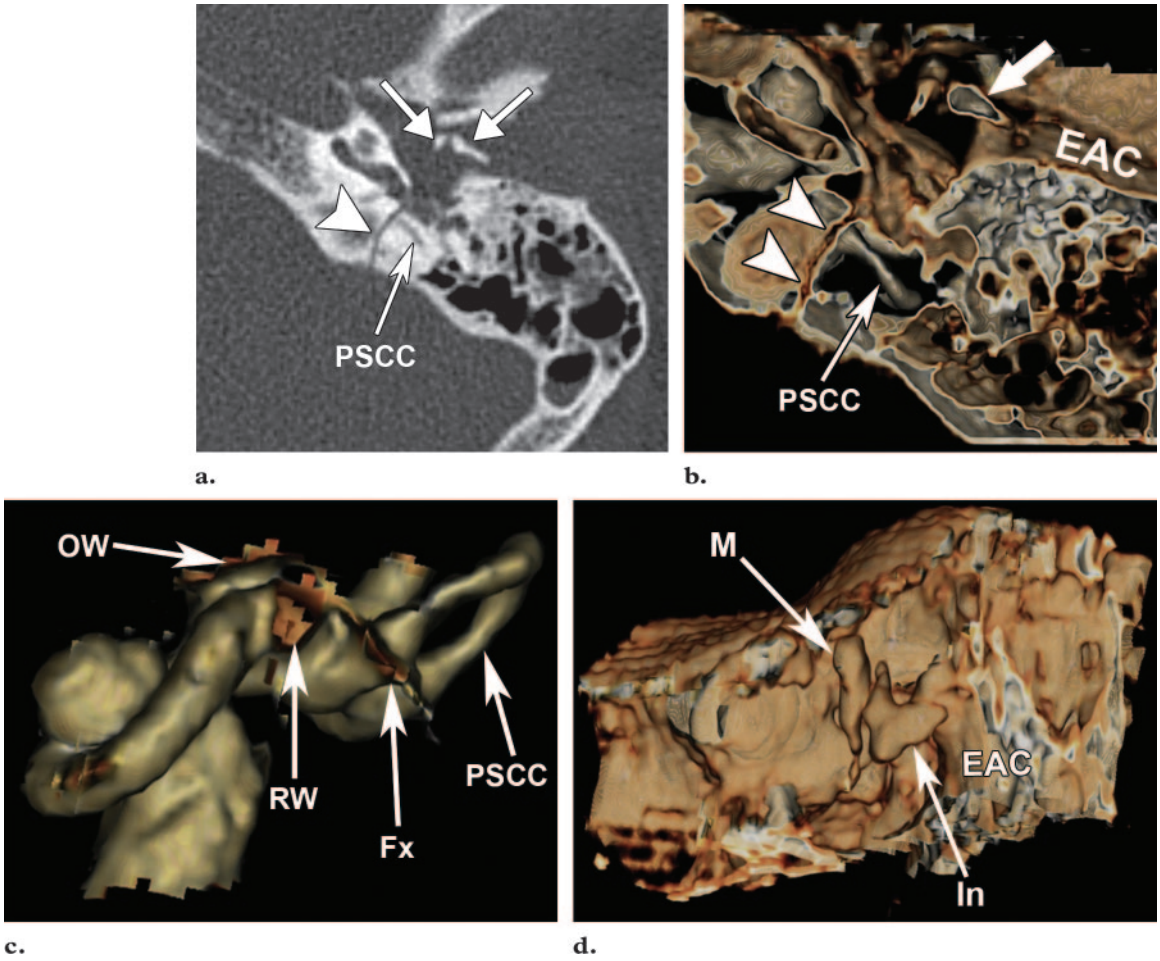

Figure 20. Temporal bone fracture caused by trauma in a 51-year-old man. **(a)** CT scan shows a fracture (arrowhead) through the posterior semicircular canal *(PSCC)* extending to involve the ossicles (arrows). **(b)** Corresponding 3D CT reformatted image also demonstrates the fracture (arrowheads) through the base of the posterior semicircular canal *(PSCC)* extending to the ossicles. The ossicles appear to have an abnormal configuration, suggesting possible dislocation of one of the ossicles (arrow) into the external auditory canal *(EAC)*. **(c)** Three-dimensional VR CT image (posteroinferior view) shows the fractured bony labyrinth, with the fracture line *(Fx)* extending through the base of the posterior semicircular canal *(PSCC)* into the round window *(RW)* and oval window *(OW)*. **(d)** Three-dimensional VR CT image (anterior view after dissection of the anterior wall of the EAC) shows incudomalleolar disarticulation, with the incus *(In)* located lateral to the malleus *(M)* and partly within the external auditory canal *(EAC)*.

Trauma

Fractures of the temporal bone can be categorized into three types—longitudinal, transverse, or mixed—on the basis of their orientation relative to the long axis of the petrous temporal bone. Fractures that run parallel to the long axis are classified as longitudinal fractures, whereas those that run perpendicular to the long axis are classified as transverse fractures. Longitudinal fractures are more common than transverse fractures. Longitudinal fractures cross the middle ear and are often associated with ossicular dislocation. Transverse fractures traverse the fundus of the IAC or the bony labyrinth, resulting in sensorineural hearing loss (8,10,38,39). Although temporal bone fractures can usually be identified on conventional 2D scans, their complete extent is best appreciated on 3D reformatted images (6).

Figure 20 illustrates the role of 3D MPR CT images in evaluating the extent of temporal bone fractures. In this case, extension of the fracture line into the region of the oval and round windows was easily seen on the 3D CT reformatted

images (Fig 20b, 20c) but only retrospectively on the conventional CT scans (Fig 20a). In addition, the ability to rotate the 3D reformatted images in space allowed more complete evaluation of the associated ossicular dislocation. The characteristic shape of the most laterally positioned ossicle on 3D reformatted images proved that it was the incus, not the malleus as would normally be expected, that was dislocated. This incudomalleolar dislocation was not appreciated on the 2D CT scans alone. Furthermore, because the fracture line extended into the region of the oval window (which was better seen on the 3D VR CT image), it is possible that, despite undergoing ossicular reconstruction, the patient may continue to experience a degree of hearing deficit from potential scar formation at the oval window fracture site. Thus, 3D CT reformatted images can also help predict the degree of functional recovery expected after surgery.

Conclusions

In this article, we have discussed and illustrated the role of 3D CT reformation in evaluating both the normal anatomy and pathologic conditions of the temporal bone. The ability to rapidly reformat these images in multiple projections and manipulate their spatial orientation allows more detailed evaluation of the temporal bone anatomy, including its microanatomic structures, and of related disease entities.

References

1. Reisser C, Schubert O, Forsting M, Sartor K. Anatomy of the temporal bone: detailed three-dimensional display based on image data from high-resolution helical CT—a preliminary report. Am J Otol 1996;17(3):473–479.
2. Calhoun PS, Kuszyk BS, Heath DG, Carley JC, Fishman EK. Three-dimensional volume rendering of spiral CT data: theory and method. RadioGraphics 1999;19(3):745–764.
3. Jun BC, Song SW, Cho JE, et al. Three-dimensional reconstruction based on images from spiral high-resolution computed tomography of the temporal bone: anatomy and clinical application. J Laryngol Otol 2005;119(9):693–698.
4. Chuang MT, Chiang IC, Liu GC, Lin WC. Multidetector row CT demonstration of inner and middle ear structures. Clin Anat 2006;19(4):337–344.
5. Isono M, Murata K, Aiba K, Miyashita H, Tanaka H, Ishikawa M. Minute findings of inner ear anomalies by three-dimensional CT scanning. Int J Pediatr Otorhinolaryngol 1997;42(1):41–53.
6. Howard JD, Elster AD, May JS. Temporal bone: three-dimensional CT. II. Pathologic alterations. Radiology 1990;177(2):427–430.
7. Rodt T, Ratiu P, Becker H, et al. 3D visualization of the middle ear and adjacent structures using reconstructed multi-slice CT datasets, correlating 3D images and virtual endoscopy to the 2D cross-sectional images. Neuroradiology 2002;44(9):783–790.
8. Curtin HD, Sanelli PC, Som PM. Temporal bone: embryology and anatomy. In: Som PM, Curtin HD, eds. Head and neck imaging. 4th ed. St Louis, Mo: Mosby, 2003; 1062–1075.
9. Williams PL, Warwick R, Dyson M, Bannister LH, eds. Gray's anatomy. 37th ed. New York, NY: Churchill Livingstone, 1989; 1219–1243.
10. Swartz JD, Harnsberger HR, eds. Imaging of the temporal bone. 2nd ed. New York, NY: Thieme, 1992.
11. Donaldson JA, Duckert LG, Lambert PM, Rubel EW. Surgical anatomy of the temporal bone. 4th ed. New York, NY: Raven, 1992.
12. Lemmerling MM, Stambuck HE, Mancuso AA, Antonelli PJ, Kubilis PS. CT of the normal suspensory ligaments of the ossicles in the middle ear. AJNR Am J Neuroradiol 1997;18(3):471–477.
13. Yamada M, Tsunoda A, Muraoka H, Komatsuzaki A. Three-dimensional reconstruction of the incudostapedial joint with helical computed tomography. J Laryngol Otol 1999;113(8):707–709.
14. Lemmerling M, Vanzieleghem B, Dhooge I, Van Cauwenberge P, Kunnen M. CT and MRI of the semicircular canals in the normal and diseased temporal bone. Eur Radiol 2001;11(7):1210–1219.
15. Hamamoto M, Murakami G, Kataura A. Topographical relationships among the facial nerve, chorda tympani nerve and round window with special reference to the approach route for cochlear implant surgery. Clin Anat 2000;13(4):251–256.
16. Rubinstein D, Sandberg EJ, Cajade-Law AG. Anatomy of the facial and vestibulocochlear nerves in the internal auditory canal. AJNR Am J Neuroradiol 1996;17(6):1099–1105.
17. Fatterpekar GM, Mukherji SK, Lin Y, Alley JG, Stone JA, Castillo M. Normal canals at the fundus of the internal auditory canal: CT evaluation. J Comput Assist Tomogr 1999;23(5):776–780.
18. Fatterpekar GM, Mukherji SK, Alley J, Lin Y, Castillo M. Hypoplasia of the bony canal for the cochlear nerve in patients with congenital sensorineural hearing loss: initial observations. Radiology 2000;215(1):243–246.
19. Tuccar E, Tekdemir I, Aslan A, Elhan A, Deda H. Radiological anatomy of the intratemporal course of facial nerve. Clin Anat 2000;13(2):83–87.
20. Valvassori GE, Clemis JD. The large vestibular aqueduct syndrome. Laryngoscope 1978;88(5):723–728.
21. Lane JI, Witte RJ, Driscoll CL, Camp JJ, Robb RA. Imaging microscopy of the middle and inner ear. I. CT microscopy. Clin Anat 2004;17(8):607–612.

22. Berrettini S, Forli F, Bogazzi F, et al. Large vestibular aqueduct syndrome: audiological, radiological, clinical, and genetic features. Am J Otolaryngol 2005;26(6):363–371.
23. Lai CC, Shiao AS. Chronological changes of hearing in pediatric patients with large vestibular aqueduct syndrome. Laryngoscope 2004;114(5):832–838.
24. Arcand P, Desrosiers M, Dube J, Abela A. The large vestibular aqueduct syndrome and sensorineural hearing loss in the pediatric population. J Otolaryngol 1991;20(4):247–250.
25. Zeifer B, Sabini P, Sonne J. Congenital absence of the oval window: radiologic diagnosis and associated anomalies. AJNR Am J Neuroradiol 2000; 21(2):322–327.
26. Swartz JD, Glazer AU, Faerber EN, Capitanio MA, Popky GL. Congenital middle-ear deafness: CT study. Radiology 1986;159(1):187–190.
27. Booth TN, Vezina LG, Karcher G, Dubovsky EC. Imaging and clinical evaluation of isolated atresia of the oval window. AJNR Am J Neuroradiol 2000;21(1):171–174.
28. Lambert PR. Congenital absence of the oval window. Laryngoscope 1990;100(1):37–40.
29. Yi Z, Yang J, Li Z, Zhou A, Lin Y. Bilateral congenital absence of stapes and oval window in 2 members of a family: etiology and management. Otolaryngol Head Neck Surg 2003;128(6):777–782.
30. Koesling S, Kunkel P, Schul T. Vascular anomalies, sutures and small canals of the temporal bone on axial CT. Eur J Radiol 2005;54(3):335–343.
31. Kojima H, Miyazaki H, Yoshida R, et al. Aberrant carotid artery in the middle ear: multislice CT imaging aids in diagnosis. Am J Otolaryngol 2003; 24(2):92–96.
32. McElveen JT Jr, Lo WW, el Gabri TH, Nigri P. Aberrant internal carotid artery: classic findings on computed tomography. Otolaryngol Head Neck Surg 1986;94(5):616–621.
33. Lo WW, Solti-Bohman LG, McElveen JT Jr. Aberrant carotid artery: radiologic diagnosis with emphasis on high-resolution computed tomography. RadioGraphics 1985;5(6):985–993.
34. Gaurano JL, Joharjy IA. Middle ear cholesteatoma: characteristic CT findings in 64 patients. Ann Saudi Med 2004;24(6):442–447.
35. El-Bitar MA, Choi SS, Emamian SA, Vezina LG. Congenital middle ear cholesteatoma: need for early recognition—role of computed tomography scan. Int J Pediatr Otorhinolaryngol 2003;67(3): 231–235.
36. Park K, Moon SK, Cho MJ, Won YY, Baek MG. 3D micro-CT images of ossicles destroyed by middle ear cholesteatoma. Acta Otolaryngol 2004; 124(4):403–407.
37. Jang CH, Wang PC. Preoperative evaluation of bone destruction using three-dimensional computed tomography in cholesteatoma. J Laryngol Otol 2004;118(10):827–829.
38. Meriot P, Veillon F, Garcia JF, et al. CT appearance of ossicular injuries. RadioGraphics 1997; 17(6):1445–1454.
39. Lee D, Honrado C, Har-El G, Goldsmith A. Pediatric temporal bone fractures. Laryngoscope 1998; 108(6):816–821.

This article meets the criteria for 1.0 credit hour in category 1 of the AMA Physician's Recognition Award. To obtain credit, see accompanying test at http://www.rsna.org/education/rg_cme.html.

Role of 3D CT in the Evaluation of the Temporal Bone

Girish M. Fatterpekar, MD, et al

RadioGraphics 2006; 26:S117–S132 • **Published online** 10.1148/rg.26si065502 • **Content Codes:** CT HN NR

Page S118
During initial postprocessing, we observed that any amount of gantry tilt on the CT scanner caused distortion of 3D CT reformatted images. Therefore, 2D CT scans were obtained with a 0• gantry tilt and a scanning plane parallel to the inferior orbitomeatal line. In addition, overlapping submillimeter reconstruction of the raw data was performed to obtain the best possible 3D CT reformatted images.

Page S120
The surface area of the tympanic membrane is up to 30 times greater than that of the oval window. Thus, the pressure exerted on the tympanic membrane by a sound wave is concentrated through the ossicles onto the much smaller area of the oval window, resulting in a pressure increase and amplification of sound transmission. A lever mechanism that exists between the ossicles further contributes to sound amplification.

Page S126
A dilated vestibular aqueduct can be easily recognized at conventional cross-sectional imaging by identifying its abnormal size in relation to the adjacent posterior semicircular canal. However, 3D multiplanar reformatted (MPR) CT images can more clearly demonstrate the classic funnel-shaped deformity of the dilated vestibular aqueduct, which occurs due to an enlarged endolymphatic sac housed within the dorsal vestibular aqueduct (Fig 16) (8).

Page S126
Recent advances in imaging techniques, such as submillimeter reconstruction and 3D VR multiplanar imaging, have markedly improved the evaluation of congenital anomalies that cause conductive hearing loss. To obtain the best possible surgical outcome, it is vital for the neuro-otologist or otolaryngologist to appreciate the full extent of congenital anomalies present. It is therefore imperative that the radiologist demonstrate the underlying anomalies in the greatest possible detail, thereby allowing optimal presurgical planning.

Pages S129
There are various types of surgeries for the treatment of cholesteatomas, including simple, modified radical, and radical mastoidectomies. The type of surgery performed depends on the extent of disease, which is directly related to the extent of the underlying erosions. Therefore, detailed preoperative radiologic assessment of the cholesteatoma is important (8,37).